Reactions of Etched, Single Crystal (111)B-Oriented InP To Produce Functionalized Surfaces with Low Electrical Defect Densities

Marcel Sturzenegger, Nicholas Prokopuk, C. N. Kenyon, William J. Royea, and Nathan S. Lewis*

Division of Chemistry and Chemical Engineering, Noyes Laboratory, California Institute of Technology, Pasadena, California 91125

Received: July 8, 1999

Synthetic routes have been developed that allow attachment of a variety of functional groups to etched, single-crystal InP surfaces. Benzyl halides, alkyl halides, silyl halides, and esters reacted readily with InP to yield covalently attached overlayers on the semiconductor surface. High-resolution X-ray photoelectron spectroscopy (XPS) revealed that the functionalization chemistry was consistent with the reactivity of surficial hydroxyl groups. Analysis of the XP spectra of the (111)B-oriented (P-rich) face in ultrahigh vacuum revealed signals ascribable to a monolayer of oxidized P atoms on the etched (111)B InP surface. The lack of reactivity of the (111)A-oriented (In-rich) face with these same functionalization reagents is therefore attributed to the difference in the nucleophilicity and acidity of the In and P oxides that are present on the (111)A and (111)B faces, respectively. The coverage of benzylic groups obtained through functionalization of (111)B-oriented InP with benzyl halides was estimated to be 4×10^{14} cm^2. This coverage implies that the functionalization can only proceed at alternate surface P atom sites in this system, which is expected from molecular packing considerations of these particular functional groups. Photoluminescence decay measurements were performed to investigate the electrical properties of the etched and modified InP surfaces, and these data indicated that the surface recombination velocity of the functionalized InP surface was $\approx 10^2$ cm s^{-1}. This low surface recombination velocity implies that <1 electrically active defect is present for every 10^5 atoms on the modified InP surface, indicating that high electrical quality can be maintained while introducing a variety of chemical functionalities onto the (111)B surface of InP.

I. Introduction

One of the major goals in the area of semiconductor electrochemistry is to achieve molecular-level control over the physical, chemical, and electrical properties of semiconductor surfaces. For some semiconducting solids, such as GaAs, improved methods to control the surface characteristics are crucial because the highly defective properties of the native GaAs surface preclude fabrication of entire classes of electrical and optical devices. For other semiconductors, such as Si and InP, the native or deliberately oxidized surfaces have electrical properties that are satisfactory for many device applications.[1,2] Nevertheless, control over the surface chemistry of these solids is still a notable goal because as devices become smaller, the surface properties will play an increasingly important role in determining the overall device behavior. In addition, procedures to improve adhesion of metals, to limit oxidation, or to inhibit corrosion on such surfaces would be very useful in certain device applications. Synthetic strategies that allow the introduction of chemical functionality onto such semiconductor surfaces, without introducing significant levels of electrical defects, are therefore highly desirable.

In this work, we describe an apparently general synthetic strategy for the functionalization of InP surfaces. InP is a useful target for surface modification because its direct optical band gap and its high electron mobility make InP a material of choice in several optoelectronic technologies.[1,3−5] In many types of device applications, however, InP yields unsatisfactory performance because the lack of chemical control over the electrical properties of the InP surface prevents fabrication of the desired device structures and interfaces. For example, improved semiconductor/metal Schottky barriers could be obtained if Fermi level pinning could be prevented on InP surfaces.[1,6] Additionally, improved metal-oxide-semiconductor field-effect transistors could be obtained if suitable chemical control were achieved over the chemistry of InP surfaces. The InP/native oxide interface has been shown to have a low surface recombination velocity in contact with air ambients,[7−9] so oxide/hydroxide functionalities on this surface might be useful starting reagents for effecting modification of this semiconductor without inducing a concomitant degradation in the electrical properties of the resulting devices.

Previous studies of InP surface chemistry have mostly emphasized oxide growth and passivation reactions.[10,11] Little effort has been directed toward functionalizing this surface with molecular reagents while maintaining a high degree of electrical perfection. Waldeck and co-workers have successfully modified InP surfaces using a high-temperature exposure to thiols,[12] but the chemical processes responsible for this surface modification approach have not yet been elucidated. In another approach, benzyl bromides were found to react selectively with the P-rich, (111)B orientation of InP.[13] This procedure afforded a useful route to molecular level control over the adhesion of conducting polymers onto the InP surface.[13] In a recent X-ray photoelectron spectroscopy (XPS) and chemical reactivity study, the reactivity of the P-rich (111)B InP surface with alkyl halides, benzyl halides, and silyl halides was ascribed predominantly to surface

10.1021/jp992290f CCC: $18.00
Published on Web 11/19/1999

hydroxyl moieties.[14] In this manuscript, we provide a full description of these surface reactions. We also present an electrical characterization of the resulting InP surface to facilitate comparison of the level of electrical defects of this semiconductor surface before and after the chemical functionalization steps.

II. Experimental Section

A. Chemicals. Reagent grade tetrahydrofuran (THF), methanol (CH_3OH), and acetonitrile (CH_3CN) were obtained from EM Science. The CH_3OH was dried over magnesium turnings, and a small amount of I_2 was added before distillation to facilitate the removal of water. Acetonitrile was first dried over CaH_2 and then dried over P_2O_5. The solvents were distilled from their drying agents under a dinitrogen (N_2) atmosphere and stored under N_2.

Bromine (Br_2; 99.5%) was obtained from EM Science. Boron trifluoride diethyl etherate [$(C_2H_5)_2O{\cdot}BF_3$], 4-(trifluoromethyl)-benzyl bromide (p-$CF_3C_6H_4CH_2Br$; 98%), and 4-methylbenzotrifluoride (p-$CF_3C_6H_4CH_3$; 98%) were obtained from Aldrich Chemical Company, and 4,4,4-trifluoro-1-iodobutane [$CF_3(CH_2)_3I$; bp, 126−127 °C] was obtained from Lancaster Inc. These reagents were used without any further purification. (3,3,3-Trifluoropropyl)dimethylchlorosilane [$CF_3(CH_2)_2Si(CH_3)_2Cl$; PCR, 97%] and triethylamine [$(C_2H_5)_3N$; Aldrich, 99+ %] were outgassed by 3 freeze−pump−thaw cycles prior to use.

Lithium chloride (LiCl), lithium perchlorate ($LiClO_4$), and potassium bromide (KBr) were obtained from J. T. Baker. These reagents were converted to their anhydrous form by heating for 8 h in quartz tubes at ∼250 °C under an active vacuum (2×10^{-2} Torr). Sodium hexafluoroantimonate(V) ($NaSbF_6$; 98%) was obtained from Alfa and was used as received.

InP single crystals were obtained from CrystaComm (Mountain View, CA). The (111)B-oriented wafer was n-type, whereas the (111)-oriented wafer with both A and B sides polished and the (110)-oriented wafers were doped p-type. The dopant densities were 5.5×10^{15}, 4.2×10^{18}, and 2×10^{18} cm^{-3}, respectively, as reported by the manufacturer. The surfaces were polished by the manufacturer by applying a dilute HF etch. The (111)A and (111)B faces of the wafer that had been polished on both sides were distinguished by using the "AB etch".[15] The orientation of the (110) face was verified by powder X-ray diffraction (XRD) methods.

B. Reactions. *1. Reagents.* 4-(Trifluoromethyl)benzyltriphenylphosphonium bromide (p-$CF_3C_6H_4CH_2P(C_6H_5)_3Br$) was prepared according to a general procedure given by Hauser et al.[16] A solution of 4-(trifluoromethyl)benzyl bromide (1.20 g, 5 mmol) in 20 mL of CH_3CN was added to a solution of triphenylphosphine (1.31 g, 5 mmol) in 30 mL of CH_3CN under N_2(g). The reaction mixture was stirred at 65 °C for 8 h. The amount of solvent was reduced to 40 mL under vacuum. While the solution was kept at 65 °C, *n*-hexane was added until the product started to precipitate (ca. 5 mL). After redissolving the precipitate by adding 0.5 mL of CH_3CN, the solution was slowly cooled to room temperature. The resulting crystalline product was isolated by filtration and washed four times with *n*-hexane. ^{1}H NMR ($CDCl_3$, δ): 5.8 (d, 2H), 7.3−7.9 (m, 19H).

12-Bromo-*n*-dodecyl-4-(trifluoromethyl)-benzoate (p-$CF_3C_6H_4COO(CH_2)_{12}Br$) was prepared according to a procedure described in the literature.[17] A solution of 12-bromo-1-dodecanol (1.15 g, 4.34 mmol) in 10 mL of CH_2Cl_2 was added to a solution of 4-(trifluoromethyl)benzoyl chloride (1.0 g, 4.77 mmol) and triethylamine (0.88 g, 8.7 mmol) in 10 mL of the same solvent. After the solution was stirred for 1 h at room temperature, ∼10 mL of the solvent was removed under vacuum. The solution was cooled to −5 °C to give white crystals of triethylammonium chloride that were removed by filtration. The filtrate was washed three times with water, and the product was isolated as a viscous liquid upon evaporation of the organic phase. ^{1}H NMR ($CDCl_3$, δ): 1.2−1.6 (m, 16H), 1.9 (m, 4H), 3.4 (t, 2H), 4.4 (t, 2H), 7.7 (d, 2H), 8.2 (d, 2H). *n*-Dodecyl-4-(trifluoromethyl)-benzoate (p-$CF_3C_6H_4COO(CH_2)_{11}CH_3$) was prepared in an analogous fashion by reacting the acyl chloride with 1-dodecanol. ^{1}H NMR ($CDCl_3$, δ): 0.9 (t, 3H), 1.2−1.5 (m, 18H), 1.8 (m, 2H), 4.4 (t, 2H), 7.7 (d, 2H), 8.2 (d, 2H).

General procedures to synthesize indium(III)−phosphine complexes can be found in a review by Roundhill.[18] To prepare tribromobis(tris(4-fluorophenyl)phosphine)indium(III) ($InBr_3[(C_6H_4F)_3P]_2$), a solution of tris(4-fluorophenyl)phosphine (1.0 g, 3.16 mmol) in 5 mL of anhydrous ethyl acetate was added slowly under N_2(g) to a solution of indium(III) bromide (0.545 g, 1.51 mmol) in 5 mL of the same solvent. The solution was stirred for 1 h and then warmed to 50 °C. *n*-Hexane was then added until precipitation was initiated. The precipitate was redissolved by adding 1 mL of anhydrous ethyl acetate, and the resulting solution was slowly cooled to room temperature. The product was filtered and washed four times with cold *n*-hexane (mp 180 °C). Anal. for $InBr_3[(C_6H_4F)_3P]_2$ Calcd C, 43.8, H, 2.46. Found: C, 43.7; H, 2.34.

2. InP Sample Preparation. Sample preparation was performed in a glovebox that was maintained under an inert N_2 atmosphere. Sample transfer to the XP spectrometer was also carried out under N_2(g). The samples were etched just prior to surface derivatization, and no sample was reused more than five times to avoid the possibility of increasing the surface roughness and obtaining erroneous coverage values through repeated etching of the surface.

The initial and final surfaces were characterized by XPS. Introduction of $-CF_3$ groups into the reagent was very useful because F provides the highest XP sensitivity among the nonmetallic elements and because the fluorinated carbon (C_F) yields a C 1s peak that is well separated from that of hydrocarbons or from peaks due to adventitious carbonaceous material.

3. Etching Procedures. Triangular or rhomboidally-shaped InP samples with an edge length of about 4 mm were successively immersed for 60 s in a freshly prepared, diluted Br_2 solution (0.05% in CH_3OH) and in a 4 M NH_3-CH_3OH solution. After each step, the samples were rinsed thoroughly with CH_3OH. The entire procedure was then repeated and the samples were blown dry with N_2(g). This procedure was employed for the (111)B-, (111)A-, and (110)-oriented InP samples.

4. Surface Derivatization of (111) and (110) Oriented InP. Surface derivatization reactions and related control experiments were performed using nominally identical procedures. Details of the experimental conditions used for the surface derivatization reactions are listed in Table 1. As an example of the procedures used in these reactions, freshly etched InP samples were immersed for 60 min in a 0.2 M solution of p-$CF_3C_6H_4CH_2Br$ in CH_3CN at 62 ± 3 °C. The samples were removed from the derivatization solution, thoroughly rinsed with hot (65 °C) CH_3CN, and blown dry with N_2. Similar methods were used, with modifications in the conditions as indicated, for the other reactions of Table 1.

5. Anion-Exchange Reactions. Immediately following the surface derivatization, InP samples were immersed into a 0.01 M solution of either $LiClO_4$, $NaSbF_6$, or KBr in CH_3OH. Samples were maintained in the solution for 120 min at room

TABLE 1: Parameters for Surface Derivatization Reactions of (111)- and (110)-Oriented InP Surfaces

derivatization reagent	reagent concentration (mol L^{-1})[a]	promoter	promoter concentration (mol L^{-1})	immersion time (min)[b]
		(111)B InP		
p-$CF_3C_6H_4CH_2Br$	0.2	a) none		60
	0.2	b) $(C_2H_5)_3N$	0.02	60, 120 180
p-$CF_3C_6H_4CH_3$	0.2	none		60
$CF_3(CH_2)_3I$	0.2	a) none		60, 120
	0.2	b) $(C_2H_5)_3N$	0.02	60, 120, 180
$(C_2H_5)_2O{\cdot}BF_3$	0.4	none		30
$CF_3(CH_2)_2Si(CH_3)_2Cl$	0.2	a) none		120
	0.2	b) $(C_2H_5)_3N$	0.1	60, 120, 240
p-$CF_3C_6H_4COO(CH_2)_{11}CH_3$	0.2	none		120
p-$CF_3C_6H_4COO(CH_2)_{12}Br$	0.1	none		120
		(111)A InP		
p-$CF_3C_6H_4CH_2Br$	0.2	$(C_2H_5)_3N$	0.02	120
		(110) InP		
p-$CF_3C_6H_4CH_2Br$	0.2	$(C_2H_5)_3N$	0.02	60, 120
$CF_3(CH_2)_3I$	0.2	$(C_2H_5)_3N$	0.02	60, 120

[a] Acetonitrile (CH_3CN) was used as the solvent for all reagents, except for $(C_2H_5)_2O{\cdot}BF_3$, which was dissolved in a solution of hexanes/CH_2Cl_2 (10:1). [b] Reaction temperatures were 62 ± 3 °C, except for the reaction with $(C_2H_5)_2O{\cdot}BF_3$, which was performed at 40 ± 3 °C.

temperature. After this period, the samples were removed from the solution and were thoroughly rinsed with pure CH_3OH.

C. X-ray Photoelectron Spectroscopy (XPS). *1. Experimental Procedures.* The XP spectra were recorded with an M-Probe surface spectrometer (Surface Science Instruments). The spectrometer was divided into two separate chambers. One chamber was equipped with an Ar^+ sputtering unit, a heating stage, a quadrupole mass spectrometer (VG Scientific), and a low-energy electron diffraction (LEED) system. The second chamber contained the XPS and ultraviolet photoelectron spectrometer (UPS) sources and a hemispherical analyzer. Each chamber was pumped with a cryogenic pump (CTI−Cryogenics). The base pressure during data collection was $< 5 \times 10^{-10}$ Torr. The mass spectrometer identified water vapor as the main gaseous component in the ultrahigh vacuum (UHV) chamber.

The spectrometer was connected to a glovebox via a high-vacuum load-lock. This arrangement allowed anaerobic transfer of the samples from the glovebox into the spectrometer. All spectra were recorded with focused and monochromatized Al $K\alpha_{1,2}$ irradiation ($h\nu = 1486.6$ eV), and the X-ray beam was incident on the surface at an angle of 55° with respect to the surface normal. The analyzer was also positioned at an angle of 55° with respect to the surface normal.

The Au $4f_{7/2}$ line [binding energy (BE) = 84.00 eV] from a sputter-cleaned gold foil was used to calibrate the energy scale of the spectrometer. The linearity of the energy scale was checked with a sputter-cleaned copper foil [BE(Cu $2p_{3/2}$) = 932.67 eV]. On both metals, adventitious carbon was observed at a BE of 285.0 ± 0.1 eV. The Au $4f_{7/2}$ line also provided a measure of the instrumental line width. When the gold foil was irradiated with the 400 × 1000 μm X-ray spot and the pass energy of the analyzer set at 105 eV, the full-width-at-half-maximum (fwhm) of the Au $4f_{7/2}$ line was 1.14 ± 0.01 eV. With a pass energy set at 54 eV, a fwhm of 0.90 ± 0.01 eV was observed.

All samples [except the UHV cleaved (110) InP surfaces] were irradiated with an ellipsoidal X-ray spot with dimensions of 400 × 1000 μm. The UHV-cleaved (110) InP samples were irradiated with an ellipsoidal X-ray spot of 200 × 750 μm. Survey scans (BE = 0−1000 eV) were recorded with a pass energy of 155 eV. Binding energies and chemical compositions reported in this work are based on high-resolution spectra taken with a pass energy of 105 eV. Sufficient scanning was performed to provide peak heights that were at least 5000 counts above background. A pass energy of 54 eV was used to study the P 2p region in detail.

The InP samples were affixed with gold springs onto an electrically grounded sample holder. Insulating samples were mechanically powdered in a mortar and were mounted onto double-sided adhesive tape. A fine nickel mesh was fixed ~2 mm above insulating samples.[19] During data acquisition, the static charge was neutralized with a low-energy-electron flood gun. The energy of the applied electron beam was adjusted so that the measured BEs followed the applied energy linearly and so that the fwhm values were minimal. Usually an electron beam of 3 eV was sufficient to fulfill these two conditions. Using this procedure, the peaks obtained from insulating samples were typically not >20% broader than those of conducting samples.

2. Data Analysis. To correct for charging effects, the measured BEs were referenced to the BE of adventitious carbon, which was taken to be 285.0 eV. Chemical compositions of homogeneous samples and attached overlayers were derived from normalized peak areas and from Wagner's empirically derived atomic sensitivity factors[20] for XPS. The normalized peak areas were calculated with the standard software provided with the M Probe XP spectrometer after a linear background correction had been carried out.

The surface coverage of derivatized samples can be expressed either as the overlayer−substrate intensity ratio, measured as I(F 1s)/I(In $3p_{3/2}$) (with I being the peak intensity in arbitrary units), or as an absolute coverage Γ in atoms per cm^2. The former is a semiquantitative measurement and can only be rigorously used for a comparison between samples that are derivatized with identical molecular overlayers. The absolute coverage was calculated by applying an overlayer-substrate model.[21] The models shown in Scheme 1 are based on the assumption that the molecules are oriented perpendicular to the surface, as has been observed for strongly chemisorbed molecules on metal surfaces such as *n*-alkane thiols or benzyl mercatpans on Ag (111) and Pd (111).[22] The C_4-hydrocarbon chain was assumed to possess an all-trans conformation by analogy to *n*-alkane thiols on gold[23] as well as on GaAs (100).[24] The bond lengths were taken from Allen et al.[25] Based on these assumptions, the thickness of the p-$CF_3C_6H_4CH_2$– overlayer on InP was estimated to be 8.7 Å, whereas the thickness of the $CF_3(CH_2)_3$– overlayer on InP was 6.4 Å.

Scheme 1 illustrates the model structures used for the coverage computations, in which the $-CF_3$ groups are confined

SCHEME 1: Representation of *p*-$CF_3C_6H_4CH_2$- and $CF_3(CH_2)_3$-units Bound to the (111)B InP Surface

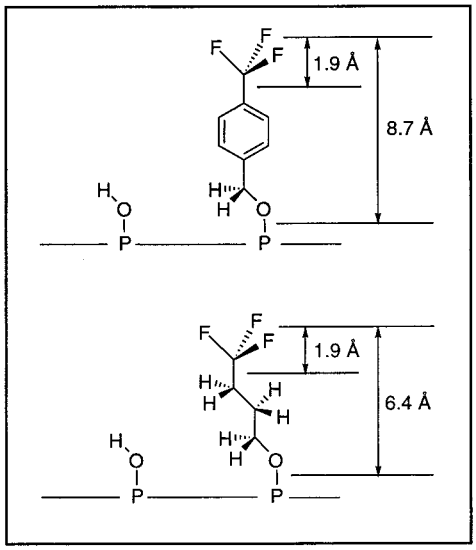

to the upper part of the overlayer. To localize the origin of the F 1s photoelectrons more precisely, the overlayer (o) was schematically divided into two sections and the $-CF_3$ layer was treated as a second overlayer (o′) with a thickness of 1.9 Å. A mathematical treatment of the two-layer-substrate model for XPS signals has been performed by Ebel.[26]

The surface coverage was then calculated using the following equations:[27,28]

$$I_{A,o'} = I_A^{\infty} \cdot n_{A,o'} \cdot \left\{1 - e^{-\frac{d_{o'}}{\lambda_A(E_A)\cdot\cos\beta}}\right\} \quad (1)$$

$$I_{B,s} = I_B^{\infty} \cdot n_{B,s} \cdot e^{-\frac{d_o}{\lambda_A(E_B).\cos\beta}} \quad (2)$$

$$\Gamma_A = \frac{n_{A,o'}}{d_{o'}} \quad (3)$$

The index A represents the element of interest in the overlayer o′, and B represents the element of interest in the substrate s. In eqs 1−3, $I_{A,o'}$ and I_B are the measured intensities of the particular core level peaks of A and B, respectively; I_A^{∞} and I_B^{∞} are the sensitivity factors (SFs) of elements A and B, respectively; n_A and n_B are the number of atoms per unit volume of elements A and B, respectively; d_o is the thickness of the entire overlayer, and $d_{o'}$ is the thickness of the $-CF_3$ layer; $\lambda_A(E_A)$ and $\lambda_A(E_B)$ are the escape depths in the overlaying material at the energies E_A and E_B, respectively; the angle β between the analyzer and the surface normal was 55° for all the measurements described herein; and Γ is the surface coverage in atoms per cm^2.

Based on the crystallographic data for InP,[29] the number density of P atoms (and of In atoms) in bulk InP was calculated to be 1.94×10^{22} cm^{-3}. An atomically perfect (111)B InP face is terminated by 6.7×10^{14} P atoms per cm^2, and the number of P atoms on a atomically perfect (110) InP surface was calculated to be 4.1×10^{14} cm^{-2}. Values for λ in the organic overlayer were derived from the work of Laibinis et al.,[30] in which the escape depth was determined for *n*-alkane thiols on group IB metals (Cu, Ag, Au) at different photoelectron energies. A quantity that is similar to λ is the inelastic mean free path (IMFP).[31] In contrast to λ, the IMFP is based on a theoretical approach and must be corrected to take into account inelastic scattering.[27] For polystyrene, the experimentally measured λ values and the theoretically derived IMFPs, corrected for inelastic scattering, agreed to within 10% (Table 2).

Equations 1−3 were used to calculate the thickness of indium phosphate overlayers on oxidized InP samples. The number density of P atoms (per cm^3) in the overlayer was taken to be the same as that in crystalline $InPO_4$; namely, 1.39×10^{22} cm^{-3}.[29] Both the escape depth of the substrate and that of the overlayer were taken to be 23 Å, as derived from the IMFP of InP.[27,32] To estimate the number of oxidized P atoms on an anaerobically etched (111)B surface, the surface P atoms and surface-bound OH groups were considered to be the overlayer. The overlayer thickness was taken to be 3.5 Å, and the escape depth was assumed to be the same as that of bulk InP; namely, 23 Å.

D. Surface Recombination Velocity Measurements. Time-resolved photoluminescence measurements were performed using a time-correlated single-photon-counting apparatus that has been described previously.[33,34] Rhodamin 6G (Exciton) was used in the dye laser to provide an excitation at 600 nm. The repitition rate was set to 152 kHz to ensure that the delay between pulses was substantially larger than the time scale for the observed InP luminescence decay (6 ms). The beam was directed onto the sample at an angle of ∼45° and was focused using a 25.4-mm focal length, diffraction-limited, achromatic lens. The incident photon flux was estimated to be 2.7×10^{13} photons cm^{-2} pulse^{-1}, indicating that the concentration of photogenerated carriers exceeded the concentration of thermally generated electrons in the lightly doped n-InP sample by >2 orders of magnitude. Under such high-level injection conditions, the influence of any residual electric field on the observed PL decay was minimized.[35] Emission corresponding to the band-to-band luminescence of InP (925 nm) was selected with a monochromator and was passed to the detection system.

The two-dimensional device simulator ToSCA[36] was used to simulate the experimentally observed PL decay curves. The software package employs Fermi−Dirac statistics and simultaneously solves Poisson's equation and the current continuity equations; a more detailed description of ToSCA has been published previously.[35,37] The excitation was approximated by a Gaussian-shaped pulse with a fwhm of 70 ps that corresponds to the system response of the experimental setup. The nonradiative bulk lifetime (240 ns) was obtained from an exponential fit of the tail of the PL decay curve at $t > 350$ ns.

Because the effect of surface-state trap saturation can become important under high-level injection conditions,[38] nonradiative recombination via surface states was simulated using a trap model[35] that treats the occupancy of recombination centers (traps) as a dynamic process. The trap model in the present case contrasts with the conventional Shockley−Read−Hall treatment that assumes steady-state conditions (i.e., no net change in the occupancy of traps). In these simulations, the rate constants for electron and hole capture were assumed to be equal (10^{-8} cm^3-s^{-1}). This value corresponds to the product of the thermal velocity of the carriers ($\upsilon_{th} = 10^7$ cm s^{-1}) and the capture cross section of the traps (typically $\sigma = 10^{-15}$ cm^2 for neutral traps). The surface traps were positioned energetically at the intrinsic Fermi level, where such states can interact with both the conduction and valence band and thus provide the most efficient centers for recombination.

III. Results

A. Reactivity of (111)B-Oriented InP Surfaces with Benzyl Bromide. Figure 1 displays the XP spectra for a (111)B-oriented InP surface before and after exposure to *p*-$CF_3C_6H_4CH_2Br$ in

TABLE 2: Escape Depths (λ),[30] Inelastic Mean Free Paths,[32] and Wagner's Empirically Derived Sensitivity Factors (SF)[48] for Some Elements of Interest

parameter	Br 3d	Si 2p	P 2p	C 1s	In $3d_{5/2}$	O 1s	I 3d	In $3p_{3/2}$
kinetic energy (eV)	1418	1385	1358	1199	1042	955	867	822
escape depth, λ (Å)[a]			38.8	35.4	31.9	30.0		27.1
corrected inelastic mean free path (Å)[b]			36.9	33.5	30			24.9
sensitivity factor, SF_{lit}[c]	0.83	0.37	0.39	0.25	3.9	0.66	6.0	1.85
sensitivity factor, SF_{exp}[d]			0.39	0.27	4.62	1.75		

[a] Escape depths in *n*-alkane thiols on group IB metals.[30] [b] Inelastic mean free path for polystyrene,[32] corrected for inelastic scattering.[27] [c] Wagner's sensitivity factors.[48] [d] Sensitivity factors derived from closely related organic compounds and single-crystal (110) InP.

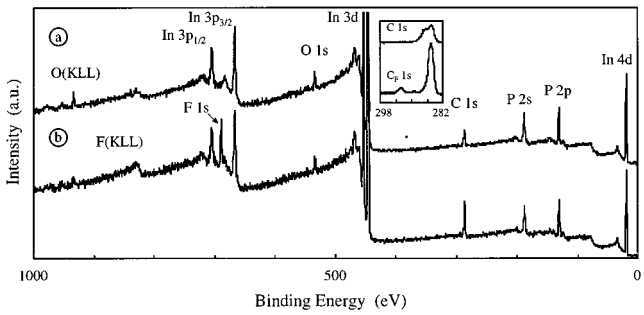

Figure 1. The XPS survey scans of anaerobically etched (111)B InP (a) before and (b) after exposure to *p*-$CF_3C_6H_4CH_2Br$. The inset magnifies the C 1s region and shows the presence of fluorinated carbon (C_F) on surfaces that had been exposed to *p*-$CF_3C_6H_4CH_2Br$.

CH_3CN. The survey scan of the etched surface displayed the expected peaks for In and P (Table 3, Figure 1a). Minor traces of Br at 69.1 eV were detectable, but the intensity of this peak varied from sample to sample. A high-resolution scan of the P 2p region of such etched samples showed no detectable quantities of phosphate at 133.3 eV.[39]

Reaction of this surface with *p*-$CF_3C_6H_4CH_2Br$ produced new XPS signals ascribable to F atoms as well as new signals ascribable to fluorinated C (C_F; Figure 1b and inset). After correction for the cross-section differences between C and F atoms, the ratio of these signals was close to the 1:3 ratio expected for a $-CF_3$ group. No detectable changes in high resolution scans of the In 3d or P 2p XPS regions were observed as a result of the surface modification process. Thus, the oxidation state of these elements remained constant in the 35 Å near-surface region that is probed by the XPS experiment at photoelectron energies of 444.5 eV (In $3d_{5/2}$) or 128.8 eV (P 2p). After surface modification, the C signal increased relative to its level on an etched surface; however, the presence of adventitious C on all samples precluded a quantitative analysis of this region of the spectrum.

Control experiments indicated that the bromide functionality in the *p*-$CF_3C_6H_4CH_2Br$ reagent was required for surface modification because negligible C_F and F XPS signals were observed on (111)B InP surfaces that had been exposed to *p*-$CF_3C_6H_4CH_3$. The C_F and F levels after reaction with *p*-$CF_3C_6H_4CH_2Br$ were essentially unchanged after thorough rinsing or exposure to clean CH_3CN for 60 min. The spectral changes depicted in Figure 1 are thus consistent with expectations for chemisorbed *p*-$CF_3C_6H_4CH_2\cdot$ groups bound to the InP surface.

B. Anion-Exchange Reactivity of the Functionalized (111)B InP Surface. After exposure to *p*-$CF_3C_6H_4CH_2Br$, the Br/F ratio in the XP spectra of (111)B-oriented InP samples was < 0.02 (Table 3). This ratio would not be expected for an alkylation reaction in which a phosphonium ion was formed because such a process requires the presence of an anion to compensate the excess positive charge that is introduced onto the InP surface. To rule out the possibility that the Br^- anion had exchanged with OH^- or with another anion during the functionalization and/or rinsing steps, (111)B InP surfaces that had been modified with *p*-$CF_3C_6H_4CH_2\cdot$ groups were subsequently exposed to solutions that contained large excesses of anions. Metathesis of a putative surface-bound anion with these other anions should produce clear signatures in the XP spectra that are characteristic of the atomic constituents of these other anionic species.

Table 3 summarizes the XPS data obtained from such surfaces after exposure to $LiClO_4$ or $NaSbF_6$, each at a concentration of 0.01 M in CH_3CN. In all cases, only traces of the atoms in the anions were detectable on the InP surface. Furthermore, rinsing the surface with pure solvent typically removed these signals to undetectable levels. Notably, rinsing the *p*-$CF_3C_6H_4CH_2Br$-treated (111)B InP surface with a KBr solution (0.01 M in CH_3CN) after surface modification also lowered the residual Br signal. This collective lack of reactivity toward anion exchange of the modified surface strongly implies that the initial functionalization reaction does not produce free or bound Br^-. These results therefore suggest that binding of the *p*-$CF_3C_6H_4CH_2-$ group does not occur through alkylation of a P lone pair on the InP surface.

C. Reactivity of Etched (111)B InP Surfaces with Alkyl Halides, Boron Trifluoride Etherate, and Silyl Halides. To characterize further the reactivity of the (111)B-oriented InP surface, etched (111)B InP samples were exposed to $CF_3(CH_2)_3I$ in CH_3CN. As shown in Figure 2 and Table 3, $CF_3(CH_2)_3I$ reacted similarly to *p*-$CF_3C_6H_4CH_2Br$ and yielded persistently bound surface alkyl groups with no evidence for concomitant formation of surface-localized iodide anions. For example, the XPS spectra of (111)B-oriented InP surfaces obtained after reaction with $CF_3(CH_2)_3I$ revealed a cross-section-corrected C_F/F ratio of 0.38 and a corrected I/F ratio of <0.14 (Table 3).

To probe the propensity of the (111)B-oriented InP surface functionality to act as a Lewis base, the etched (111)B surface was exposed to $(C_2H_5)_2O\cdot BF_3$ that had been dissolved in a solution of hexanes/CH_2Cl_2 (10:1). Only small amounts of F were detectable after exposure of (111)B-oriented InP to $(C_2H_5)_2O\cdot BF_3$. On such surfaces, the F 1s/In $3p_{3/2}$ intensity ratio was typically <0.1. Based on this value and assuming an escape depth of 15 Å and a thickness of 2.8 Å, the number of bound BF_3 groups is estimated to be $<1 \times 10^{14}$ cm^{-2}, compared with 6.7×10^{14} cm^{-2} surface P atoms on an atomically flat (111)B InP surface.

To distinguish between the presence of P lone pairs and P−OH functionalities on etched (111)B InP crystals, the reactivity of the (111)B-oriented surface was investigated with a silyl chloride reagent. Figure 3 and Table 3 present the XPS data obtained after reaction of the (111)B InP surface with $CF_3(CH_2)_2Si(CH_3)_2Cl$ in the presence of $(C_2H_5)_3N$ in CH_3CN. A monochlorosilane was chosen to prevent adventitious water

TABLE 3: XPS Peak Positions[a] and Intensities[b] of Derivatized (111) and (110) InP Surfaces

	P 2p		In $3d_{5/2}$		In $3p_{3/2}$	C_F 1s		O 1s	F 1s		X			intensity ratio	atomic ratio[c]	
derivatized surface	BE[d]	*I*	BE	*I*	BE	BE	*I*	*I*[e]	BE	*I*		BE	*I*	PO_x/InP[f]	C_F/F	X/F
(111)B InP																
anaerobically etched InP	128.7	0.29	444.5	2.75	665.8			0.17						<0.05		
InP + *p*-$CF_3C_6H_4CH_2Br$	128.6	0.31	444.4	2.82	665.7	292.6	0.027	0.18	688.2	0.26	Br 3d	68.9	<0.02	<0.05	0.41	<0.10
InP + *p*-$CF_3C_6H_4CH_3$	128.7				665.5				688.3	0.08				<0.05		
InP + *p*-$CF_3C_6H_4CH_2Br$					665.7	292.9	0.028		688.3	0.19	Cl 2p	—[g]			0.58	<0.02
then: +$LiClO_4$-CH_3OH																
InP + *p*-$CF_3C_6H_4CH_2Br$					665.5	292.7	0.029		688.2	0.25	Sb 3d	—[g]			0.46	<0.02
then: + $NaSbF_6$-CH_3OH																
InP + $CF_3C_6H_4CH_2Br$					665.6	292.7	0.029		688.2	0.22	Br 3d	68.98	0.013		0.45	0.07
then: + KBr-CH_3OH																
InP + *p*-$CF_3(CH_2)_3I$	128.8	0.29	444.5	2.64	665.7	292.6	0.018		688.2	0.19	I 3d	619.4	<0.16		0.38	<0.14
InP + $(C_2H_5)_2O{\cdot}BF_3$	128.5	0.25	444.4	2.65	665.5				688.5	0.1				<0.05		
InP + $CF_3(CH_2)_2Si(CH_3)_2Cl/(C_2H_5)_3N$	128.6	0.30	444.4	2.73	665.8	292.7	0.015		688.4	0.25	Si 2p	102.0	0.027	<0.05	0.46	0.56
InP + $CF_3C_6H_4COO(CH_2)_{11}CH_3$	128.5	0.25	444.4	2.89	665.8	292.8	0.028		688.3	0.25	Br 3d	—[g]		<0.05	0.44	
InP + *p*-$CF_3C_6H_4COO(CH_2)_{12}Br$	128.5	0.24	444.5	2.86	665.7	293.1	0.026		688.5	0.23	Br 3d	69.0	<0.03	<0.05	0.45	<0.16
InP + *p*-$CF_3C_6H_4CH_2Br/(C_2H_5)_3N$	128.9	0.28	444.5	2.68	665.8	292.7	0.033		688.2	0.39	Br 3d	69.0	<0.03	<0.05	0.34	<0.10
(111)A InP																
anaerobically etched InP	128.8	0.22	444.6	2.75	665.9			0.23						<0.02		
InP + *p*-$CF_3C_6H_4CH_2Br/(C_2H_5)_3N$					665.9				688.42	<0.01				<0.02		
(110) InP																
anaerobically etched InP	128.6	0.22	444.5	2.63	665.8			0.16						<0.05		
InP + *p*-$CF_3C_6H_4CH_2Br/(C_2H_5)_3N$	128.6	0.24	444.6	2.56	665.9	292.8	0.018		688.3	0.20	Br 3d	69.2	<0.04	<0.05	0.36	<0.24
InP + $CF_3(CH_2)_3I/(C_2H_5)_3N$	128.7	0.21	444.6	2.48	665.8	292.8	0.013		688.3	0.12	I 3d	619.5	0.10	<0.05	0.43	<0.19

[a] Peak positions were obtained with a peak-fitting procedure and are referenced against C 1s = 285.0 binding eV. Values are from repeated experiments and are reported as averaged binding energies (BE). Standard deviations in all cases were <0.1 eV. [b] Intensities were referenced to the In $3p_{3/2}$ signal after normalization with respect to scan duration and background subtraction. [c] Atomic ratios were derived from the measured XPS intensities (see e.g., Seah[27]). Sensitivity factors were taken from Wagner et al.[48] and are listed in Table 2. [d] P 2p binding energy measured at maximum peak height. [e] Intensity of convoluted peaks with maxima at 533.0 ± 0.3 eV. [f] PO_x represents indium phosphate with a BE of 133.3 eV. [g] No signal detectable above background.

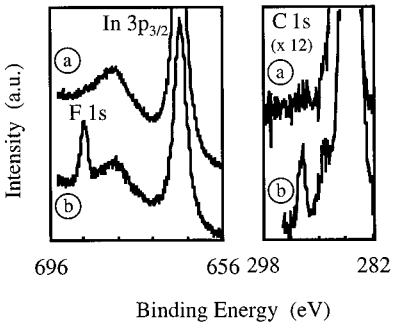

Figure 2. The XPS spectra of a (111)B InP surface (a) before and (b) after exposure to $CF_3(CH_2)_3I$.

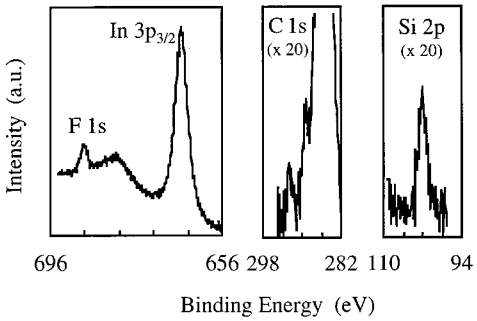

Figure 3. The XP spectra of a (111)B InP surface after exposure to $CF_3(CH_2)_2Si(CH_3)_2Cl$.

from cross-linking the silane reagent and from forming an insoluble polymer that might be confused with the formation of persistently bound chemisorbed silyl groups. The $(C_2H_5)_3N$ was required to facilitate the surface reaction, as is the case for reaction of Si−OH groups with chlorosilanes.[40] As depicted in Figure 3, exposure of the (111)B-oriented InP surface to $CF_3(CH_2)_2Si(CH_3)_2Cl$ produced persistently bound F, C_F, and Si signals in the ratios expected for a $-Si(CH_3)_2(CH_2)_2CF_3$ fragment on the InP surface. Negligible signals for atoms of the anions were detectable on the functionalized surface. The F, C_F, and Si signals were robust and were not affected by various solvent rinses or by boiling in CH_3CN or CH_3OH. Si−P bonds are very weak and unstable in alcoholic solutions, and would not be expected to withstand the reaction conditions.[41] In contrast, silyl halides react readily with −OH groups, forming strongly bound −O−Si−R linkages that could account for the observed functionalization.

D. Reactivity of Etched (111)B−Oriented InP Surface with Esters. To support the hypothesis that −OH groups dominate the reactivity of (111)B-oriented InP surfaces, reactions with esters were investigated. Reaction with *p*-$CF_3C_6H_4COO(CH_2)_{11}CH_3$ yielded persistently bound $-CF_3$ groups on the surface, as shown by the cross-section-corrected C_F/F ratio of 0.44 measured in the XP spectrum of modified surfaces (Table 3). In addition, the F/In XP signal ratio was extremely close to that found for the reaction of (111)B InP with *p*-$CF_3C_6H_4CH_2Br$. This similarity implies that the alkyl chain had been removed by the reaction, otherwise the differences in the thickness of the overlayers would have produced different F/In signal ratios for the same ratio of atoms in the overlayer. Strong evidence for cleavage of the ester was obtained from reaction of (111)B InP surfaces with *p*-$CF_3C_6H_4COO(CH_2)_{12}Br$. Reactions with this ester yielded essentially identical F/In ratios in the XPS spectra as were obtained after the reactions with *p*-$CF_3C_6H_4CH_2Br$ or with *p*-$CF_3C_6H_4COO(CH_2)_{11}CH_3$. Furthermore, all such reactions produced negligible Br signals in the XPS scans. The lack of a Br signal after reaction with the *p*-$CF_3C_6H_4COO(CH_2)_{12}$-Br ester, along with the reactivity of *p*-$CF_3C_6H_4COO(CH_2)_{11}CH_3$, indicates that the functionalization chemistry occurs at the ester group as opposed to at the primary alkyl carbon center. Cleavage of esters is a well-known quantitative analysis for −OH functionalities,[42] and this type of surface reaction is fully consistent with the presence of hydroxyl groups as the dominant chemically reactive species on the etched (111)B InP surface.

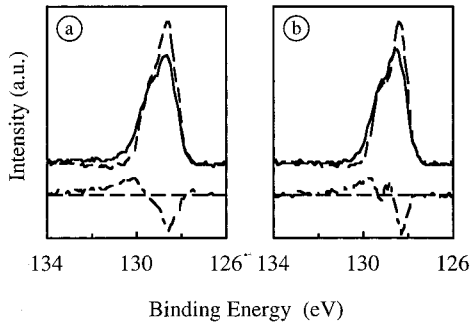

Figure 4. The XP spectra of the P 2p region for various InP samples: (a) solid line, etched (111)B InP; dashed line, etched (111)A InP; (b) solid line, etched (110) InP; dashed line, (110) InP cleaved in UHV. The dotted lines are difference spectra for the signals in each panel, in each case showing the presence of additional, high-binding-energy signals for the etched (111)B and etched (110) surfaces. The peaks were normalized with respect to their area after a linear background subtraction.

E. High-Resolution XPS Data for Anaerobically Etched (111)B-Oriented, (111)A-Oriented, (110)-Oriented, and UHV−Cleaved (110)-Oriented InP Surfaces. To obtain spectral-based evidence for the presence of −OH functionalities on the etched (111)B InP surface, high-resolution XP spectra for etched (111)B and (110) InP surfaces were carefully compared with those of etched (111)A and UHV-cleaved (110)-oriented InP surfaces. The latter two surfaces should have reduced levels of oxidized surface P atoms and should serve as references for analysis of the line shapes of the XPS data arising from the etched and functionalized (111)B-oriented InP surfaces.

Figure 4a displays the high-resolution XPS data in the P 2p region of an anaerobically etched (111)A-oriented InP surface. This figure also displays the difference spectrum between the XPS spectrum of this surface and that of the anaerobically etched (111)B-oriented InP surface. The signal for the (111)A surface could be well fit by a single Gaussian/Lorentzian doublet, in accord with expectations for the instrumental line shape and detector response function. In contrast, the XP spectrum of the etched (111)B surface displayed a shoulder to the high binding energy side of the main P 2p signal. The difference spectrum indicated that this peak had a binding energy of 130.0 eV, which is consistent with expectations for the peak position of oxidized P atoms. A P 2p XPS peak with a similar binding energy was also observed in the difference spectrum of anaerobically etched (110)-oriented InP relative to the spectrum of UHV-cleaved (110)-oriented InP surfaces (Figure 4b). The estimated coverage of the surface species in the high-binding-energy peak was 8.8×10^{14} cm^{-2}. The contribution of the high-binding-energy peak to the entire P 2p peak was determined to be (13 ± 3)%, and the estimated coverage of the surface species was 3.4×10^{14} cm^{-2}. Because the density of P surface atoms on an ideal (111)B surface is 6.7×10^{14} atoms cm^{-2}, this observation indicates that ~50% of the surface P atoms are oxidized on the etched (111)B-oriented InP surface, even when the etching process is performed under nominally anaerobic conditions in a N_2(g)-purged glovebox.

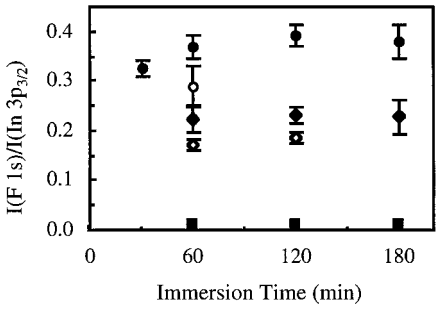

Figure 5. Intensity ratios F 1s/In $3p_{3/2}$ as a function of time for (111) InP exposed to *p*-$CF_3C_6H_4CH_2Br$ (○), *p*-$CF_3C_6H_4CH_2Br/(C_2H_5)_3N$ (●), $CF_3(CH_2)_3I$ (◇), $CF_3(CH_2)_3I/(C_2H_5)_3N$ (♦), and (111)A InP exposed to *p*-$CF_3C_6H_4CH_2Br/(C_2H_5)_3N$ (B). The intensity ratios are averaged values from at least 5 samples with the error bars representing 1σ values.

F. Coverage of *p*-$CF_3C_6H_4CH_2$ Groups on Anaerobically Etched (111) InP Surfaces. The observation that $(C_2H_5)_3N$ promotes the reaction of (111)B-oriented InP surfaces with $CF_3(CH_2)_2Si(CH_3)_2Cl$ prompted us to investigate whether an amine also affected the reactivity of (111)B-oriented InP surfaces toward benzyl and alkyl halides. The XP spectra indicated that the presence of $(C_2H_5)_3N$ indeed led to substantially higher amounts of F on derivatized surfaces; for example, for surfaces exposed to *p*-$CF_3C_6H_4CH_2Br$ and reaction times of 60 min, the calculated coverage increased by 30% (Table 3) if $(C_2H_5)_3N$ was added to the solution.

To quantify the differences in reactivity between the anaerobically etched (111)B and (111)A faces of InP, the reaction of *p*-$CF_3C_6H_4CH_2Br$ with both crystal faces was monitored as a function of time. The intensity ratios between the measured F 1s and In $3p_{3/2}$ XPS signals are displayed in Figure 5. The reaction of (111)B-oriented surfaces with *p*-$CF_3C_6H_4CH_2Br$ showed saturation behavior, as expected for a surface reaction. The limiting coverage of *p*-$CF_3C_6H_4CH_2$ groups was calculated to be 4.3×10^{14} cm^{-2}, as compared with a calculated P atom density of 6.7×10^{14} cm^{-2} on a perfect (111)B-oriented surface. To evaluate the variation of the calculated coverage as a function of the sensitivity factors, escape depths, and the chosen core level in the overlayer and substrate, the limiting coverage was calculated with two sets of SF and λ values (Table 4) and with six pairs of core levels. Table 5 summarizes the results of this analysis. The variation is dominated by the chosen core level pairs. With pairs that included the C_F 1s peak instead of the corresponding F 1s peak, the calculated coverage was always higher (Table 5). The averaged limiting coverage based on pairs with C_F 1s signals was calculated to be 0.80, whereas core level pairs including the F 1s signal yielded a limiting coverage of 0.58. The variation within the two groups introduced by different sensitivity factors and escape depths was ± 0.1.

In contrast to the P-rich (111)B-oriented InP surfaces, In-rich (111)A-oriented InP surfaces that had been exposed to *p*-$CF_3C_6H_4CH_2Br$ yielded negligible F signals in the XP spectrum. The cross-section-corrected intensity ratio of the F 1s/In $3p_{3/2}$ signals on such surfaces was independent of the reaction time and was always <0.01. The coverage of *p*-$CF_3C_6H_4CH_2^-$ groups on this surface was estimated to be $< 3.4 \times 10^{13}$ cm^{-2}.

Analysis of the coverage of (111)B-oriented InP surfaces that had been exposed to $CF_3(CH_2)_3I$ also revealed saturation behavior. For reaction times >60 min, the F 1s/In $3p_{3/2}$ intensity ratio was 0.22 ± 0.01. The limiting coverage of $CF_3(CH_2)_3^-$ groups was calculated to be 2.9×10^{14} cm^{-2}.

G. Reactivity of Aerobically Etched (111)B InP Surfaces. To investigate the consequences of exposure to air on the composition and reactivity of (111)-oriented InP surfaces, (111)B-oriented InP surfaces that were etched under anaerobic conditions were exposed to air for 10 min and then investigated by XPS. The XP spectra of these surfaces displayed a distinct signal in the P 2p region at a binding energy of 133.3 eV (Figure 6a). The binding energy of this signal is in accord with literature data[39] and with our own measurements for the peak position of oxidized P in $InPO_4$. A numerical analysis of the intensity ratio of oxidized to unoxidized P signals on this surface indicates that ~50% of the surface P atoms were oxidized to $InPO_4$ during air exposure (Table 6). The intentionally oxidized samples were then exposed to *p*-$CF_3C_6H_4CH_2Br$ in CH_3CN. The resulting XP spectra (Figure 6b) revealed the presence of $-CF_3$ groups at a coverage that was very close to the one obtained from reaction of *p*-$CF_3C_6H_4CH_2Br$ with anaerobically etched (111)B-oriented InP surfaces.

Curiously, the spectra of the P 2p region of such modified surfaces displayed essentially complete removal of the phosphate signals (Figure 6b, right panel). Extended exposure to air before surface modification increased the amount of phosphate initially present on the InP surface, although the overlayer growth eventually would presumably terminate with additional exposure time due to the passivating nature of the oxide. Such heavily oxidized surfaces still, however, were observed to react with *p*-$CF_3C_6H_4CH_2Br$. In this case, though, the derivatization reaction yielded lower coverages and phosphate removal was incomplete (Table 6).

To investigate the chemistry involved in the dissolution of the phosphate overlayer, intentionally oxidized InP surfaces were exposed to either $(C_2H_5)_3N{\cdot}HBr$ in CH_3CN, $(C_2H_5)_3N$ in CH_3CN, or pure CH_3CN. Surface analysis revealed that only $(C_2H_5)_3N{\cdot}HBr$ removed the phosphate, whereas $(C_2H_5)_3N$ and CH_3CN exposure did not produce any detectable changes in the surface composition (Table 6). This observation provides an explanation for the reaction of *p*-$CF_3C_6H_4CH_2Br$ with oxidized (111)B-oriented InP because the HBr that is liberated during the reaction can etch the InP oxide and thereby produce the same surface that is obtained by anaerobic etching alone.

H. Reactivity of Etched (110)-Oriented InP Surfaces. To test the derivatization strategy for surfaces other than (111)B InP, (110) oriented InP was exposed to *p*-$CF_3C_6H_4CH_2Br$ and $CF_3(CH_2)_3I$. Both reactions yielded surfaces with persistently bound $-CF_3$ groups as shown by the cross-section corrected C_F/F ratios (Table 3). For (110) surfaces that were exposed to *p*-$CF_3C_6H_4CH_2Br$, the intensity ratio F 1s/In $3p_{3/2}$ was 0.20 ± 0.01 and the coverage with *p*-$CF_3C_6H_4CH_2^-$ was calculated to be 2.3×10^{14} cm^{-2}. Surfaces that were reacted with $CF_3(CH_2)_3I$ yielded a F 1s/In $3p_{3/2}$ intensity ratio of 0.12 ± 0.02 and the density of $CF_3(CH_2)_3^-$ groups was calculated to be 1.6×10^{14} cm^{-2}.

I. Recombination Velocity of Etched versus Functionalized (111)B InP Surfaces. Time-resolved photoluminescence methods were used to compare the electrical properties of etched InP surfaces with those of functionalized InP surfaces. Native InP has a relatively low surface recombination velocity, $S \approx 10^2$ cm s^{-1},[7-9] so the decay kinetics of photogenerated electron−hole pairs are usually dominated by the nonradiative processes in the bulk of such samples. However, for short optical penetration depths of the incident light, increases in S will produce diagnostic decreases in the observed luminescence lifetime.[35] The luminescence decay kinetics therefore allow a convenient comparison of the electrical quality of etched InP

TABLE 4: Experimentally Determined Sensitivity Factors (SF_{exp})[a]

	P 2p		C 1s		In $3d_{5/2}$		In $3p_{3/2}$	
substance	SF_{exp}	SF_{exp}/SF_{lit}	SF_{exp}	SF_{exp}/SF_{lit}	SF_{exp}	SF_{exp}/SF_{lit}	SF_{exp}	SF_{exp}/SF_{lit}
Teflon (exp)			0.255	1.02				
Teflon (lit)			0.25	1.00[b]				
$(C_4H_9)_4PF_6$ (exp)	0.356	0.91						
$AgPF_6$ (lit)	0.359	0.92[b]						
p-$CF_3C_6H_4CH_2P(C_6H_5)_3Br$	0.335	0.86	0.273	1.09				
$InBr_3[P(C_6H_4F)_3]_2$	0.341	0.87			4.62	1.19	2.10	1.13
InF_3 (exp)					5.03	1.29	2.20	1.19
InF_3 (lit)					4.68	1.20[b]		
(110) InP, powder								
(111)B InP, single crystal								
(110) InP, single crystal								

[a] SF_{exp} were derived from measured areas, after a linear background subtraction and correction for stoichiometric coefficients. As in Wagner's set of sensitivity factors (SF_{lit}), the area of the F 1s signal serves as a reference. [b] These ratios were calculated with the originally measured areas and therefore they should equal 1.

TABLE 5: Variation of the Calculated Surface Coverage, Γ, for (111)B InP Exposed to p-$CF_3C_6H_4CH_2Br$ Derived from Measured XPS Intensities with Two Sets of Sensitivity Factors and Escape Depths, Respectively

		surface coverage,[a] calculated			
ratio	int. ratio	w/λ[b] & SF_{lit}[d]	w/λ & SF_{exp}[e]	w/corr IMFP[c] & SF_{lit}	w/corr IMFP & SF_{exp}
I(F 1s)/I(In $3p_{3/2}$)	0.38	0.64	0.61	0.57	0.53
I(F 1s)/I(In $3d_{5/2}$)	0.143	0.55	0.65	0.50	0.59
I(F 1s)/I(P 2p)	1.43	0.60	0.60	0.54	0.54
I(C_F 1s)/I(In $3p_{3/2}$)	0.0335	0.89	0.78	0.96	0.70
I(C_F 1s)/I(In $3d_{5/2}$)	0.0126	0.77	0.84	0.71	0.78
I(C_F 1s)/I(P 2p)	0.126	0.84	0.77	0.78	0.72

[a] Number of p-$CF_3C_6H_4CH_2-$ groups referenced to the number of surface P atoms. [b] Escape depths in n-alkane thiols on group IB metals.[30] [c] Inelastic mean free path for polystyrene,[49] corrected for inelastic scattering.[27] [d] Wagner's sensitivity factors.[48] [e] Sensitivity factors derived from closely related organic compounds and single-crystal (110) InP.

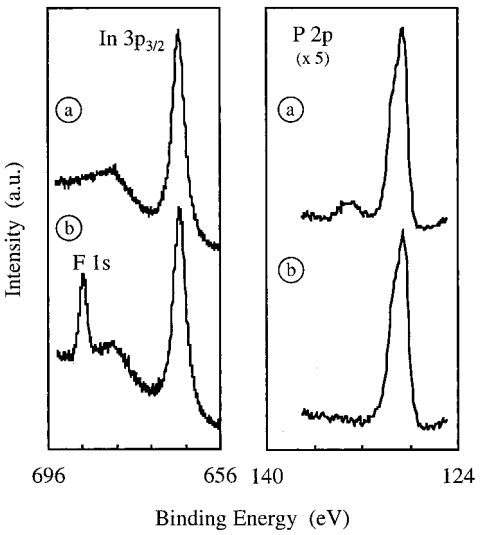

Figure 6. The XPS spectra of anaerobically etched (111)B-oriented InP surfaces (a) after exposure to air and (b) after subsequent exposure to p-$CF_3C_6H_4CH_2Br$ in CH_3CN.

surfaces with those that have been deliberately functionalized with organic groups.

Figure 7 depicts the luminescence decay kinetics for etched and modified InP surfaces. The observed luminescence decays for InP surfaces that had been modified with p-$CF_3C_6H_4CH_2Br$ were very similar to those of etched InP samples. Both surfaces had relatively low surface recombination velocities, with $S \approx 10^2$ cm s^{-1} for each system. These data were collected under high-level injection conditions to minimize any influence of changes in equilibrium band-bending arising from the surface modification process on the measurement of the surface recombination properties. Using the relationship $S = N_t\, \sigma\, \upsilon_{th}$,[1] where N_t is the density of surface traps, σ is the cross section for carrier capture (typically 10^{-15} cm^2 for neutral traps), and υ_{th} is the thermal velocity of carriers in the solid (10^7 cm s^{-1}), a value of $S = 10^2$ cm s^{-1} corresponds to $N_t \approx 10^{10}$ cm^{-2}. Because the density of atoms on an InP surface is on the order of 10^{15} cm^{-2}, a value of $N_t = 10^{10}$ cm^{-2} implies that under these conditions only 1 in every 10^5 surface atoms is an effective electrical trapping site on the chemically modified InP surface.

IV. Discussion

The etched InP surfaces investigated in this work produced survey scan XP spectra that were remarkably close to those expected for a 1:1 In/P stoichiometry, with negligible XPS signal intensity detected for other elements, except for signals ascribable to adventitious carbonaceous material. InP typically has a significant overlayer of oxidation products (often oxide and phosphates were observed) after exposure to oxidizing etches and/or exposure to air, but such oxidation was not observed using the etching and handling methods described herein. The anaerobic etching process thus offers a reproducible, near-stoichiometric starting surface for chemical modifications of this semiconductor.

The reactions investigated herein confirm the pronounced differences observed previously by Spool et al.[13] with regard to the relative reactivity of the (111)B (P-rich) and (111)A (In-rich) InP surfaces toward alkylating reagents. This differential reactivity has been used to suggest that the reactivity of the etched (111)B face is due to lone pairs on the P atoms that would be exposed on an atomically perfect (111)B surface.[13] Many of the reactions observed in this work, however, are not characteristic of P lone pairs, but are instead indicative of the presence of hydroxyl groups on the (111)B-oriented InP surface (Scheme 2). The lack of reactivity of the (111)B-oriented InP surface with $(C_2H_5)_2O{\cdot}BF_3$, the facile cleavage of esters by this

TABLE 6: XPS Data of Air-Exposed (111)B-Oriented InP Surfaces

surface	$I(InPO_4)/I(InP)^a$	Γ_{InPO_4} (cm^{-2})	$\Gamma_{InPO_4}/\Gamma_P{}^b$	I(F 1s)/I(In $3p_{3/2}$)
anaerobically etched (111)B InP (InP)	<0.02	0.5×10^{14}	0.19	—
InP, 10 min exposed to air	0.15	3.6×10^{14}	0.53	—
then: + p-$CF_3C_6H_4CH_2Br/(C_2H_5)_3N$	<0.02	0.5×10^{14}	<0.08	0.34
InP, 60 min exposed to air	0.38	7.9×10^{14}	1.18	—
then: + p-$CF_3C_6H_4CH_2Br/(C_2H_5)_3N$	0.07	1.7×10^{14}	0.26	0.31
InP, 60 min exposed to air	0.34	7.2×10^{14}	1.08	—
then: + p-$CF_3C_6H_4CH_2Br$	0.08	2.0×10^{14}	0.30	0.25
InP, 60 min exposed to air	0.36	7.6×10^{14}	1.13	—
then:				
a) + $(C_2H_5)_3N{\cdot}HBr$-CH_3CN	0.11	2.7×10^{14}	0.40	—
b) + $(C_2H_5)_3N$-CH_3CN	0.33	7.1×10^{14}	1.06	—
c) + CH_3CN	0.34	7.2×10^{14}	1.08	—

[a] Measured in the P 2p region at 133.3 eV ($InPO_4$) and 129.6 eV (InP), respectively. [b] $InPO_4$ units referenced to the number of surface P atoms.

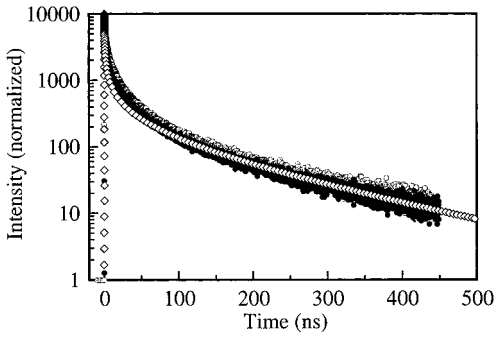

Figure 7. The PL decay curves before (○) and after (●) exposure to p-$CF_3C_6H_4CH_2Br$ and a simulated PL decay curve (◊) obtained using $S = 10^2$ cm s^{-1}.

surface, and the reaction of this surface with chlorosilanes are examples of such observations. The consistency between the various observations strongly supports the notion that hydroxyl groups are responsible for the observed surface chemistry. This conclusion results in an apparently general synthetic strategy for derivatization of the chemically etched (111)B-oriented InP surface.

The hydroxyl groups are apparently introduced during the etching and handling procedures of this surface, even though these steps were performed under nominally anaerobic conditions during the course of our study. The detailed comparison of the P 2p XPS line shapes of etched surfaces relative to the line shapes of surfaces that are prepared in UHV (Figure 4) reveals spectroscopic evidence for this surface oxidation process. X-ray standing wave (XSW) and extended X-ray absorption fine structure (EXAFS) studies have shown that surface relaxation causes only minor changes in the surface structure of UHV-cleaved (110) InP surfaces.[43,44] The differences observed between P 2p signals arising from cleaved (110)-oriented InP surfaces relative to the signals from etched (110)-oriented InP surfaces can therefore be attributed to P atoms that are chemically different from the surface or bulk P atoms of an unoxidized, cleaved InP surface. The surface relaxation of (111)B InP is less characterized, but only small changes in the surface structure have been suggested for this surface as a result of surface relaxation.[45] Thus, the differences in the XP spectra between etched (111)A and etched (111)B orientations also provide evidence of oxidized P atoms on the etched (111)B InP surface.

The presence of this oxide overlayer prior to the chemical modification step also provides a consistent explanation of why the XP spectra showed no significant change in the P oxidation state during the surface modification procedure. Changes in the P 2p region of the XP spectra would have been expected for a lone pair reactivity route because the initially neutral P species should produce a cationic P species after alkylation. Instead, in the hydroxyl group pathway, the surface P atoms are initially oxidized and no further oxidation occurs during the reaction steps of concern. The differential reactivity of the P-rich (111)B InP surface relative to the In-rich (111)A orientation can thus be ascribed to the differential chemical reactivity of the acidic −OH functionalities of P oxides relative to the basic properties expected for −OH functionalities of In oxides.

Fadley's overlayer-substrate model allows calculation of the coverage of derivatized surfaces based on measured XPS intensity data. However, the calculations depend on three parameters: SF, λ, and d_o, all of which must be determined accurately. These quantities are all difficult to obtain and can contain significant errors.[27] The XPS data for homogeneous compounds (Table 4) confirmed that XPS intensity ratios by themselves can be measured with an error of <10%. The data also show that SF values, which were computed from a regression procedure so that they could be applied to a wide range of compounds, in some cases describe the composition of particular compounds inaccurately. The data further reveal a variation in the ratio of different core levels for the same element, depending on the sample preparation. Powdered (110) InP samples yielded a In $3d_{5/2}$/In $3p_{3/2}$ ratio that agrees with ratios of other powdered samples. However, for single crystal (111) and (110) InP, this ratio is significantly higher (Table 4). We have thus derived sensitivity factors (SF_{exp}) from closely related organic compounds and single-crystal (110) InP (Table 2). An analysis of the influence of SF, λ, and the chosen core level pair on the calculated surface coverage showed that the use of different SF and λ changes the calculated coverage of these systems by <±15%. However, the choice of the overlayer core level can have a large influence on the calculated surface coverage. The C_F 1s peaks are very small and are sensitive (e.g., to convolution with shake up satellites). In contrast, F 1s peaks have intensities that are comparable with the substrate peaks and are less affected by other processes.

The results of the quantification of the coverage for (111)B and (110) InP, each derivatized with p-$CF_3C_6H_4CH_2Br$ and $CF_3(CH_2)_3I$, are listed in Table 7. The (111)B InP surface appears to accommodate a significantly larger number of molecules than does the (110) face of InP. However if the coverage is referenced instead to the number of possible reaction sites, expressed in surface P atoms per unit area, the coverage on (111)B surfaces is only slightly higher than that observed on the (110) orientation. The geometry of the (111)B face might allow a slightly denser packed overlayer, but more precise measurements would be required to address this question definitively.

SCHEME 2: Summary of the Reactivity of Etched (111)B InP Surfaces

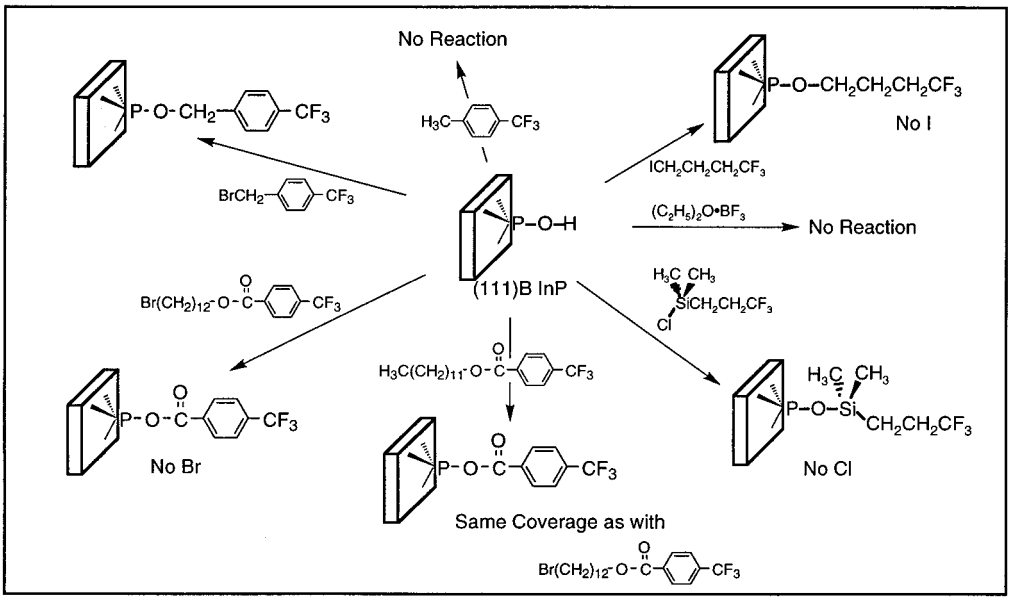

TABLE 7: Coverage of (111)B and (110) InP Surfaces

surface	I(F 1s)/I(In $3p_{3/2}$)[a]	n[b] (cm^{-2})	Γ[c]
(111)B InP + p-$CF_3C_6H_4CH_2Br/(C_2H_5)_3N$	0.38	4.3×10^{14}	0.64
	(0.03)	(0.3×10^{14})	(0.05)
(111)B InP + $CF_3(CH_2)_3I/(C_2H_5)_3N$	0.22	2.9×10^{14}	0.43
	(0.01)	(0.1×10^{14})	(0.02)
(110) InP + p-$CF_3C_6H_4CH_2Br/(C_2H_5)_3N$	0.20	2.3×10^{14}	0.55
	(0.01)	(0.1×10^{14})	(0.03)
(110) InP + $CF_3(CH_2)_3I/(C_2H_5)_3N$	0.12	1.6×10^{14}	0.38
	(0.02)	(0.3×10^{14})	(0.06)

[a] I(F 1s)/I(In $3p_{3/2}$) are averaged values from at least 5 samples, numbers in parentheses represent 1 σ values introduced by variations in the intensity ratios. [b] Number of p-$CF_3C_6H_4CH_2-$ and $CF_3(CH_2)_3-$ groups, respectively, bound to the surface. [c] Number of p-$CF_3C_6H_4CH_2-$ and $CF_3(CH_2)_3-$ groups, respectively, referenced to the number of surface P atoms.

The results show that both faces accommodate a higher number of benzyl units than hydrocarbon chains. This result is consistent with expected packing differences between the platelike benzyl units relative to the rodlike alkyl chains. The benzyl unit has a van der Waals thickness of 3.7 Å as compared with the van der Waals diameter of 4.0 Å for alkyl chains.[46] In addition, the covalent, directed bonding of hydroxyl groups on the oxidized InP surface to the alkyl overlayer will restrict the orientation angle of these overlayers much more severely than thiols on Au and therefore imposes different constraints on the alkyl chain density in the overlayer for InP surfaces than for metallic systems.

An advantage of functionalizing the surface through hydroxyl groups is that it preserves the inherently low carrier recombination velocity of the (111)B-oriented InP surface. Heller[47] has previously outlined a strategy for surface modification in which a reduction in the surface recombination velocity of a semiconductor can be achieved by inducing adsorbates to enter into strong chemical bonding with states that otherwise have energy levels in the middle of the band gap of the semiconductor. In the case of the (111)B InP surface, this approach is naturally implemented through surface oxidation because this process forms strong chemical bonds to the lone pairs on the exposed phosphorus surface atoms. In the absence of formation of these strong bonds, these lone pairs are expected energetically to serve as recombination sites. Routes to surface functionalization that do not perturb this monolayer of surface oxidation therefore should maintain the desirable electrical properties of the InP system while still offering opportunities for efficient charge transfer across the derivatized surface. The functionalization routes described herein satisfy this criterion, and thus may allow for chemical modification of surfaces with dielectric layers for controlling electron-transfer reactions, forming metal−insulator−semiconductor structures, and inhibiting surface-corrosion processes without destroying the desirable electrical properties of the InP surface. Because the functionalization route is versatile and is chemically straightforward, the approach should afford a promising strategy for preparing improved optical and electronic devices from InP. Efforts to exploit these desirable properties in actual devices are in progress and will be reported in a separate manuscript.

Acknowledgment. We acknowledge the Department of Energy, Office of Basic Energy Sciences, for support of this work. M.S. acknowledges the Swiss National Science Foundation for a postdoctoral fellowship, and we thank A. Rice for technical assistance with the XPS measurements.

References and Notes

(1) Sze, S. M. *Physics of Semiconductor Devices*, 2nd ed.; Wiley: New York, 1981.
(2) Heller, A. *ACS Symp. Ser.* **1981**, *146*, 57.
(3) Sze, S. M. *Semiconductor Sensors*; Wiley: New York, 1994.
(4) *Indium Phosphide and Related Materials: Processing, Technology and Devices*; Katz, A., Ed.; Artech House: Boston, 1992.
(5) Adachi, S. *Physical Properties of III−V Semiconductor Compounds InP, InAs, GaAs, GaP, InGaAs, and InGaAsP*; John Wiley and Sons: New York, 1992.
(6) Newman, N.; Kendelewicz, T.; Bowman, L.; Spicer, W. E. *Appl. Phys. Lett.* **1985**, *46*, 1176.

(7) Bothra, S.; Tyagi, S.; Ghandhi, S. K.; Borrego, J. M. *Solid-State Electron*. **1991**, *34*, 47−50.
(8) Brillson, L. J.; Shapira, Y.; Heller, A. *Appl. Phys. Lett*. **1983**, *43*, 175.
(9) Casey, H. C., Jr.; Buehler, E. *Appl. Phys. Lett*. **1977**, *30*, 247−249.
(10) Koval, C. A.; Austermann, R. L.; Turner, J. A.; Parkinson, B. A. *J. Electrochem. Soc*. **1985**, *132*, 613−623.
(11) Oskam, G.; Bart, L.; Vanmaekelbergh, D.; Kelly, J. J. *J. Appl. Phys.* **1993**, *74*, 3238−3245.
(12) Gu, Y.; Lin, Z.; Butera, R. A.; Smentkowski, V. S.; Waldeck, D. H. *Langmuir* **1995**, *11*, 1849−1851.
(13) Spool, A. M.; Daube, K. A.; Mallouk, T. E.; Belmont, J. A.; Wrighton, M. S. *J. Am. Chem. Soc.* **1986**, *108*, 3155−3157.
(14) Sturzenegger, M.; Lewis, N. S. *J. Am. Chem. Soc.* **1996**, *118*, 3045−3046.
(15) Thiel, F. A.; Barns, R. L. *J. Electrochem. Soc.: Solid State Science and Technology* **1979**, *126*, 1272−1274.
(16) Hauser, C. F.; Brooks, T. W.; Miles, M. I.; Raymond, M. A.; Butler, G. B. *J. Org. Chem.* **1963**, *28*, 372−379.
(17) Putvinski, T. M.; Schilling, M. L.; Katz, H. E.; Chidsey, C. E. D.; Mujsce, A. M.; Emerson, A. B. *Langmuir* **1990**, *6*, 1567−1571.
(18) Roundhill, D. M. *J. Inorg. Nucl. Chem*. **1971**, *33*, 3367−3373.
(19) Bryson, C. E., III *Surf. Sci*. **1987**, *189/190*, 50−58.
(20) Wagner, C. D.; Gale, L. H.; Raymond, R. H. *Anal. Chem*. **1979**, *51*, 466.
(21) Fadley, C. F. *Progr. Solid State Chem.* **1976**, *11*, 265−343.
(22) Gui, J. Y.; Stern, D. A.; Frank, D. G.; Lu, F.; Zapien, D. C.; Hubbard, A. T. *Langmuir* **1991**, *7*, 955−963.
(23) Nuzzo, R. G.; Korenic, E. M.; Dubois, L. H. *J. Chem. Phys*. **1990**, *93*, 767.
(24) Nakagawa, O. S.; Ashok, S.; Sheen, C. W.; Mårtensson, J.; Allara, D. L. *Jpn. J. Appl. Phys.* **1991**, *30*, 3759−3762.
(25) Allen, F. H.; Kennard, O.; Watson, D. G.; Brammer, L.; Orpen, A. G.; Taylor, R. *J. Chem. Soc., Perkin Trans. 2* **1987**, S1−S19.
(26) Ebel, M. F. *J. Electron Spectrosc. Relat. Phenom*. **1978**, *14*, 287−322.
(27) Seah, M. P. Quantification of AES and XPS. In *Practical Surface Analysis*; 2nd ed.; Briggs, D., Seah, M. P., Eds.; John Wiley & Sons: Chichester, 1990; Vol. 1; pp 201−255.
(28) Hochella, M. F., Jr.; Carim, A. H. *Surf. Sci*. **1988**, *197*, L260−L268.
(29) Pies, W.; Weiss, A. *Crystal Structure Data of Inorganic Compounds*; Springer-Verlag: Berlin, 1979; Vol. 7.
(30) Laibinis, P. E.; Bain, C. D.; Whitesides, G. M. *J. Phys. Chem.* **1991**, *95*, 7017−7021.
(31) Jablonski, A. *Surf. Interface Anal*. **1989**, *14*, 659−685.
(32) Tanuma, S.; Powell, C. J.; Penn, D. R. *Surf. Interface Anal*. **1991**, *17*, 927−939.
(33) Ryba, G. N.; Kenyon, C. N.; Lewis, N. S. *J. Phys. Chem.* **1993**, *97*, 13814−13819.
(34) Kenyon, C. N.; Tan, M. X.; Kruger, O.; Lewis, N. S. *J. Phys. Chem. B* **1997**, *101*, 2850−2860.
(35) Anz, S. J.; Kruger, O.; Lewis, N. S.; Gajewski, H. *J. Phys. Chem. B* **1998**, *102*, 5625−5640.
(36) Gajewski, H. *GAMM (Ges. Angew. Math. Mechanik) Mitteilungen* **1993**, *16*, 35.
(37) Kruger, O.; Jung, C.; Gajewski, H. *J. Phys. Chem*. **1994**, *98*, 12653−12662.
(38) Kauffman, J. F.; Balko, B. A.; Richmond, G. L. *J. Phys. Chem.* **1992**, *96*, 6371−6374.
(39) Hollinger, G.; Bergignat, E.; Joseph, J.; Robach, Y. *J. Vac. Sci. Technol., A* **1985**, *3*, 2082−2088.
(40) Tripp, C. P.; Veregin, R. P. N.; Hair, M. L. *Langmuir* **1993**, *9*, 3518−3522.
(41) Armitage, D. A. Organosilicon Derivatives of Phosphorus, Arsenic, Antimony, and Bismuth. In *The Silicon/Herteroatom Bond*; Patai, S., Rappoport, Z., Eds.; John Wiley & Sons: Chichester, 1991.
(42) Cheronis, N. D.; Ma, T. S. *Organic Functional Group Analysis*; Interscience: New York, 1964.
(43) Woicik, J. C.; Kendelewicz, T.; Miyano, K. E.; Richter, M.; Boulding, C. E.; Pianetta, P.; Spicer, W. E. *Phys. Rev. B* **1992**, *46*, 9869.
(44) Woicik, J. C.; Kendelewicz, T.; Miyano, K. E.; Richter, M.; Karling, B. A.; Bouldin, C. E.; Pianetta, P.; Spicer, W. E. *J. Vac. Sci. Technol., A* **1992**, *10*, 2041−2045.
(45) Hou, X.; Dong, G.; Ding, X.; Wang, X. *Chin. Phys. Lett*. **1986**, *3*, 545−548.
(46) Dean, J. A. *Lange's Handbook of Chemistry*; McGraw-Hill: New York, 1992.
(47) Heller, A. Chemical Control of Surface and Grain Boundary Recombination in Semiconductors. In *Photoeffects at Semiconductor-Electrolyte Interfaces*; Nozik, A. J., Ed.; American Chemical Society: Washingtion, DC, 1981; Vol. 146; pp 57−77.
(48) Wagner, C. D.; Davis, L. E.; Zeller, M. V.; Taylor, J. A.; Raymond, R. H.; Gale, L. H. *Surf. Interface Anal*. **1981**, *3*, 211−225.
(49) Tanuma, S.; Powell, C. J.; Penn, D. R. *Surf. Interface Anal*. **1993**, *21*, 165−176.